Corrections for On-Orbit ATMS Lunar Contamination

Hu Yang and Fuzhong Weng

***Abstract*—The cold calibration count from the Advanced Technology Microwave Sounder (ATMS) space view increases when the lunar radiation intrudes its antenna field of view (FOV). This increase is referred to as lunar contamination since the cold count is not matched with the specified brightness temperature of 2.73 K. For ATMS, it is found that the elapse time of lunar intrusion (LI) and the magnitude of the cold count increase are channel dependent. If the lunar-affected calibration counts are rejected in the processing, a data gap can be shown in brightness temperature at all channels. At ATMS channels 1 and 2, which have a large FOV, the LI can result in an increase of 40 counts in cold calibration. At higher frequency channels which have a smaller FOV size, the LI intensity is much stronger and can be as large as a few hundred counts. The LI becomes significant when its radiation appears in the ATMS antenna main beam. In the current ATMS operational calibration algorithm, the cold count anomaly is detected when the intensity of LI exceeds a certain threshold. The lunar radiation can be also corrected in the ATMS calibration. In doing so, a lunar radiation term is derived as a function of antenna gain, the solid angle of the Moon, and the brightness temperature of the Moon disk. This algorithm is applied in an ATMS calibration system developed at NOAA and shows a successful removal of all the lunar contamination on the earth-scene brightness temperature.**

***Index Terms*—Advanced Technology Microwave Sounder (ATMS), calibration, contamination, lunar intrusion (LI).**

I. Introduction

THE Advanced Technology Microwave Sounder (ATMS) is a total power radiometer, and its onboard calibration is achieved by viewing the cold space and an internal blackbody target, as shown in Fig. 1. In particular, there are four cold space calibration beam groups located at 76.7°, 80.0°, 81.7°, and 83.4°, respectively, from the nadir (figure is labeled with respect to the supplement angle). Within each beam group, the cosmic background radiation is also sampled four times consecutively, with each sample spaced 1.11° apart, which are referred to as SPV1, SPV2, SPV3, and SPV4. SPV1 is the closest to the Earth, and SPV4 is the closest to the satellite platform. In the current ATMS operation, cold space views at the 83.4° beam group are selected to be used in calibration. More details about ATMS instrument can be obtained from the recent studies [1], [2].

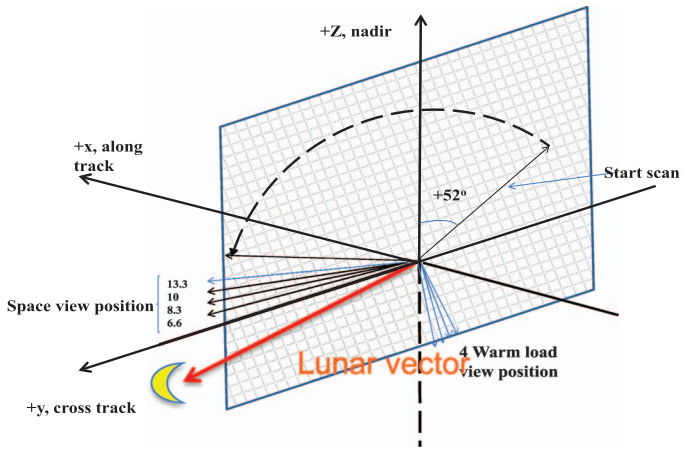

Fig. 1. ATMS scan geometry showing the positions of Earth, space, and warm calibration views. The lunar vector is also plotted in the $Y-Z$ plane. Angles of space view positions labeled in the figure are the start angles of the four space view beam groups, counting from the positive y-direction. In current operational ATMS calibration, space view samples within the 6.6° beam group are used.

In ATMS operational TDR data sets, LI can be identified by the quality flag defined as "Moon in the view." To maintain consistency, in this study, an LI event is defined as the phase wherein the edge of the Moon starts to enter the ATMS FOV of space view. After the launch of the Suomi National Polar-orbiting Partnership (NPP) satellite into orbit, it was observed that the LI happened several times a year within several consecutive orbits. Since the lunar surface brightness temperature can vary from 120 to 380 K [3]–[5] and is much higher than the cosmic background temperature of 2.7 K used in calibration, the lunar radiation can seriously impact the calibration accuracy if it is not corrected. According to the study by Kigawa and Mo, for the Advanced Microwave Sounding Unit-A (AMSU-A), which is the ATMS's predecessor, the lunar contamination showed a maximum jump of 40 counts and can produce an error of 1.5 K, for a brightness temperature of 150 K, in channels 1 and 2, over the ocean. Based on the AMSU space view observations collected during LI events, they also developed a lunar correction model [6]. Since the ATMS sampling rate and integration time is only 18 ms and is much shorter compared to the AMSU's integration time of 156 ms, the characteristics of ATMS space view observations are different from that of AMSU-A. Unlike AMSU, ATMS is a continuous slewing instrument and collects the four space view samples within every 8/3 seconds of the scan cycle. In addition, the antenna pattern features (3-dB beam width and main beam efficiency) of ATMS

Manuscript received January 14, 2014; revised October 5, 2014, July 19, 2015, and September 7, 2015; accepted October 7, 2015. Date of publication November 13, 2015; date of current version March 9, 2016. This work was supported by the National Oceanic and Atmospheric Administration's Joint Polar Satellite System Program. The views expressed in this publication are those of the authors and do not necessarily represent those of NOAA.

H. Yang is with the Earth System Science Interdisciplinary Center, University of Maryland, College Park, MD 20740 USA (e-mail: huyang@umd.edu).

F. Weng is with the NOAA Center for Satellite Applications and Research, College Park, MD 20740 USA.

Digital Object Identifier 10.1109/TGRS.2015.2490198

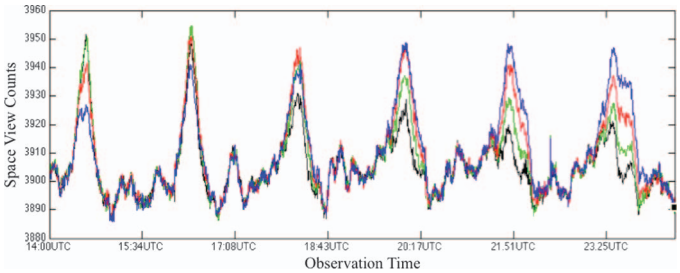

Fig. 2. Space view (SV) counts of ATMS channel 1 for an LI event occurring at 22:00–23:59 UTC on April 19, 2013. The receiver output voltage signals for observation of cold sky at four different scan positions are plotted as a function of time. The line with different colors represents space views (SV) at different positions. Black: SV1; Green: SV2; Red: SV3; Blue: SV4.

channels are also different from those of AMSU-A, which has a 3.3° beam width. Therefore, the new model is needed for the ATMS lunar contamination correction. Our research is an extension of the work by Kigawa and Mo, but with some improvements on the LI identification algorithm and correction algorithm. In this paper, ATMS data with lunar contamination information were collected since its launch on October 28, 2011. Section II explains the new algorithm that is used to detect the lunar contamination. A correction algorithm is then developed in Section III. The impacts of lunar contamination correction on the improvements of ATMS antenna temperature calibration were discussed in Section IV. A summary and conclusions are presented in the final section.

II. Identification of Lunar Contamination

A. Model of ATMS Space View Signal

For a total power radiometer such as ATMS, its cold calibration count C_c is generally written as a sum of cosmic background $C_{\rm cosmic}$, LI $C_{\rm moon}$, variation of gain C_G, and a random fluctuating component C_n from radiometer electronics and $C_{\rm sb}$ from the antenna sidelobe. At a time of t and an instrument status of p, we have

$$C_c(t,p) = C_{\rm cosmic} + C_{\rm moon} + C_G + C_n + C_{\rm sb}. \quad (1)$$

Fig. 2 displays space view counts of ATMS channel 1 at an LI case occurring at 14:00–23:59 UTC on April 19, 2013. As shown in the figure, whenever there are LIs in observations (UTC 14:00 to 15:00), the four SPV samples at each scan deviated with each other. By contrast, when there is no LI or the impacts of LI are negligible (UTC 15:00 to 16:00), the four SPV samples are identical and only fluctuated with gain. This indicates that, when the Moon entered the space view FOV, the receiver outputs are overlapped signals of lunar radiation, random noise, and normal fluctuation of receiver gain on the 2.7-K cosmic background brightness temperature. In general, the cosmic background microwave radiation is independent of scan angle and should not change with time, and thus, $\boldsymbol{C_{\rm cosmic}}$ at all four space view positions should be identical. For a periodically calibrated total power microwave radiometer such as ATMS, it is reasonable to assume that the receiver gain is kept unchanged during the 72-ms space view sampling time from SPV1 to SPV4. Considering the fact that the magnitude of receiver noise signal $\boldsymbol{C_n}$ is small, and the differences of $C_{\rm sb}$

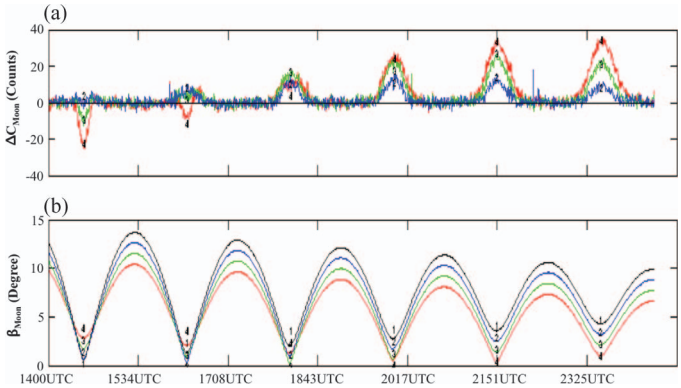

Fig. 3. (a) Identified lunar contamination signal: the vertical coordinate is the difference of receiver output space view counts; the horizontal coordinate is time of observations. (b) Corresponding separation angle between different space views and lunar vectors at ATMS channel 1. Numbers labeled in the lines represent different positions of space view.

for the four different cold space samples are ignorable, then the lunar radiation $\boldsymbol{C_{\rm moon}}$ becomes the only possible term that results in a significant difference in cold counts at four space view positions. From (1), it can be expected that the relative increase in the cold count from LI can be identified by taking one of the four space view counts (SPV1, in this case) as a reference. Fig. 3(a) shows the difference of cold counts among the four space view samples, taking the SPV1 as a reference. In a normal calibration cycle without lunar contamination, the cold counts at four different positions should be similar in mean magnitude, and the instant difference is attribute to the random noise. When the Moon appears in the FOVs of space view, the cold counts at four SPV sampling positions deviate from each other, and the magnitude of count difference $\Delta C_{\rm moon}$ depends on the intensity of lunar contamination. Since the intensity of LI at the four SPV positions is different and will change with the satellite positions in orbit, $\Delta C_{\rm moon}$ can be positive or negative.

B. Lunar Contamination Identification

For on-orbit correction of LI, the lunar-contaminated SPV signals should be identified first. As shown in Fig. 3(b), there is a close correlation between the Moon angle and LI, i.e., LI happens only when the separation angle between the SPV vector and the Moon vector are less than a certain value. The correlation between LI and SPV–Moon angle can be further explained through the lunar observation geometry and ATMS antenna pattern. As illustrated in Fig. 4, the position of Sun, Moon, and space view are plotted as three vectors overlapping on the antenna pattern. Θ is the separation angle between the Sun and the Moon, which determine the Moon phase and physical temperature of the Moon [7]; β is the separation angle between the Moon vector and the space view vector. When the antenna points to the space view direction, the peak of the antenna pattern should be aligned with the SPV vector. It is known from previous study that, for most of the ATMS channels, the sidelobe of the antenna pattern is lower than -30 dB [8]; therefore; the lunar contamination turns out to be significant only when the lunar radiation intrudes in the main beam of the antenna pattern. For a reference, the main beam efficiency and beam width for all ATMS channels are computed from the

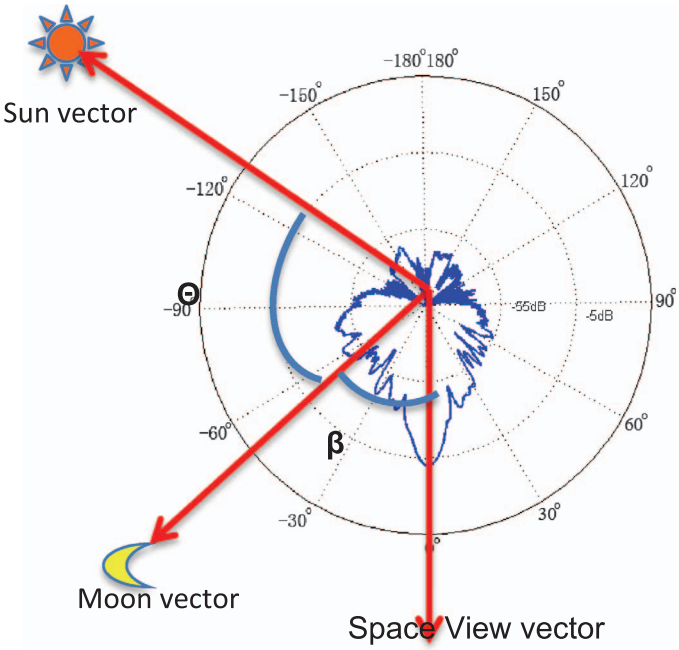

Fig. 4. Schematic diagram shows the lunar contamination when the radiation from the Moon is received through the antenna main beam. The blue curve corresponds to the ATMS antenna pattern at 23.8 GHz in the polar coordinate system.

TABLE I
ANTENNA BEAM WIDTH AND MAIN BEAM EFFICIENCY AT A FEW SELECTED ATMS CHANNELS

Freq (GHz)	Main Beam Width θ_{3dB}(deg)	Main Beam Efficiency η_{Me}(%)
23.8	5.25	96.4
31.4	5.35	97.6
50.3	2.20	97.2
54.4	2.15	97.4
57.29	2.20	98.2
88.2	2.05	95.6
165.5	1.16	**96.9**
176.3	1.10	**96.7**
183.3	1.10	**95.2**
190.3	1.07	**94.5**

ground-measured antenna pattern data, and their values at selected channels are listed in Table I [9]. Based on the aforementioned analysis, a metric for LI detection can be defined as follows:

$$0 \leq \beta' \leq 1.25 \cdot \theta_{3\ \mathrm{dB}} \tag{2}$$

where $\beta' = |\beta - \alpha_l|$, $\theta_{3\ \mathrm{dB}}$ is the main beam width listed in Table I, and α_l is the apparent angle of the Moon and is calculated as

$$\alpha_l = \frac{r_{\mathrm{moon}}}{d_{\mathrm{moon}}}$$

where $r_{\mathrm{moon}} = 1737.92$ km and is the radius of the Moon, and d_{moon} is the distance between the satellite and the Moon, which varies with satellite position in orbit. The parameters Θ, β, and d_{moon} can be obtained from satellite position and attitude measurements by using a geolocation algorithm. With the metric established earlier, the lunar-contaminated cold counts can then be identified and extracted from the SPV data sets. Fig. 5 shows the differences between the maximum and minimum values of cold counts, at channel 1, for each scan. Note that, for this channel, since LI impacts all four SPVs, the count values shown in the plot are the maximum relative magnitude of LI. Note that there are three different FOV sizes in 22 ATMS channels and the feature of lunar contamination varies from channel to channel. Fig. 6(a)–(c) shows the magnitude and

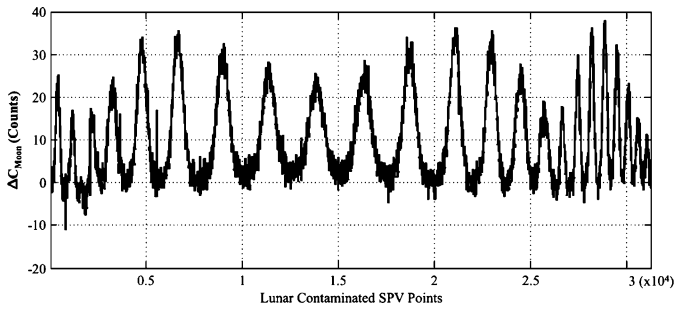

Fig. 5. Derived signals (the difference between the maximum and minimum values of cold counts for each scan) reflecting the lunar contamination at ATMS channel 1, during one full cycle of an LI event occurring from 14:00 UTC, April 19 to 01:00 UTC, April 21, 2013.

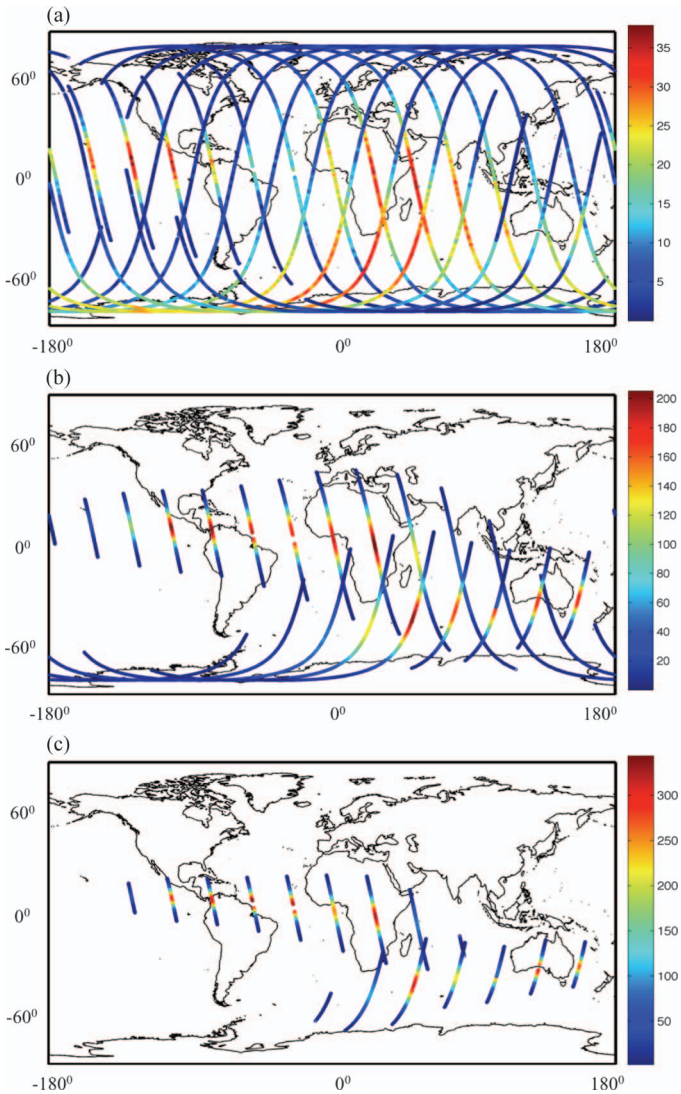

Fig. 6. Global distribution and magnitude in cold calibration count from lunar contamination at ATMS channels. (a) Channels 1 and 2, (b) channels 3–15, and (c) channels 16–22. Color bar represents the cold calibration count anomaly.

global distribution of LI at three different ATMS channels with FOV sizes equal to 5.2° (K-band), 2.2° (V-/W-bands), and 1.1° (G-band). It can be seen that the larger the FOV size, the longer the elapse time of LI. At the K-band (channels 1 and 2), the intrusion can last as long as 100 min. The maximum magnitude of LI for the K-band is about 40 counts; taking the average gain of 37.5 counts/K, about a 1-K increase is estimated for brightness temperature in cold space. The maximum lunar contaminations for the V-/W-bands (channels 3–16, 2.2° FOV) and the G-band (channels 17–22, 1.1° FOV) are 200 and 400 counts, respectively, which are equivalent to about 6- and 24-K increments in space view brightness temperature at these channels. Considering the long elapse time and strong magnitude of LI in antenna space view, a large volume of the earth scene observations might be affected by LI and become unusable; therefore, it is imperative to develop a correction algorithm to mitigate the impact of LI on ATMS on-orbit calibration.

III. Correction Algorithm for ATMS Lunar Contamination

A. Lunar Model

As described in Section II, given that all four SPV samples are contaminated, which is the worst case for ATMS space view, only the relative intensity of LI can be identified and extracted from cold counts at each scan. If $C_{\text{moon}}^{\max}$ and $C_{\text{moon}}^{\min}$ represent the LI maximum and minimum magnitudes of the SPV samples, $\Delta C_{\text{moon}} = C_{\text{moon}}^{\max} - C_{\text{moon}}^{\min}$ can be expressed in terms of the channel gain and the increased cold space view radiance ΔR_{moon} associated with LI, i.e.,

$$\Delta C_{\text{moon}} = \left[\frac{C_w - C_{c\max}}{Rw - (Rc + \Delta R_{\text{moon}}^{\max})}\right]\Delta R_{\text{moon}}^{\max} - \left[\frac{C_w - C_{c\min}}{Rw - (Rc + \Delta R_{\text{moon}}^{\min})}\right]\Delta R_{\text{moon}}^{\min} \quad (3)$$

where $C_{c\max}$ and $C_{c\min}$ are the maximum and minimum space view counts at each scan; Rw and Rc are the warm load radiance and cosmic background radiance, respectively; $\Delta R_{\text{moon}}^{\max}$ and $\Delta R_{\text{moon}}^{\min}$ are the maximum and minimum magnitudes of LI at the four space view positions, respectively, corresponding to the minimum and maximum lunar angles of β', as defined in (2).

As depicted in Section II, ΔC_{moon} in (3) can be obtained by making the difference between the maximum and minimum values of cold counts (corresponding to minimum and maximum β' angles defined in (2) at each scan). The only unknown in (3) is the LI magnitude $\Delta R_{\text{moon}}^{\max}/\Delta R_{\text{moon}}^{\min}$. From the analyses in the previous section, it is known that the magnitude of LI is closely related to the separation angle between the Moon and space view, the apparent angle of the Moon, the beam width, and the antenna pattern at a specific channel. Therefore, a physical model for ΔR_{moon} can be expressed as a function of the aforementioned factors.

For the ATMS space view, the brightness temperature increment arising from lunar contamination ΔR_{moon} can be expressed as function of antenna response function G, solid angle of the Moon Ω_{moon}, and microwave radiance of the Moon disk R_{moon}, as follows:

$$\Delta R_{\text{moon}} = G \cdot \Omega_{\text{moon}} \cdot R_{\text{moon}}. \quad (4)$$

Following the study by Mo and Kigawa, the microwave brightness temperature of the Moon disk T_{moon} can be computed from the separation angle Θ between the Moon and the Sun, as follows [7]:

$$T_{\text{moon}} = 95.21 + 104.63 \cdot (1 - \cos\Theta) + 11.62 \cdot (1 + \cos 2\Theta). \quad (5)$$

T_{moon} can then be transferred to radiance by Planck's equation. It should be noted that the aforementioned experimental expression for T_{moon} is derived under an assumption that the average emissivity of lunar surface is about 0.95, and there is no frequency dependence of brightness temperature of the Moon. Assuming that the azimuthal asymmetry is insignificant, the antenna response within the mean beam range can then be accurately simulated by a one-dimensional Gaussian function, as follows:

$$G(\beta') = \mathrm{e}^{\frac{-(\beta' - \alpha_0)^2}{2\cdot\sigma^2}}. \quad (6)$$

The normalized solid angle of the Moon in (4), i.e., Ω_{moon}, is defined as an area ratio of the full disk of the Moon and the antenna response, as follows:

$$\Omega_{\text{moon}} = \frac{\pi\left(\frac{r_{\text{moon}}}{D_{\text{moon}}}\right)^2}{\iint G(\theta,\varphi)d\theta d\varphi}. \quad (7)$$

In (6) and (7), β', β, and α_l are defined in Section II, and α_0 is an angle adjusted for offset in ATMS beam alignment. $\sigma = (0.5 \cdot \theta_{3\ \text{dB}})/\sqrt{2 \cdot \log 2}$; $\theta_{3\ \text{dB}}$ is the main beam width, as listed in Table I; r_{moon} is the radius of the Moon; D_{moon} is the distance between satellite and the Moon center.

B. Best Fitting of Model Parameters

To calculate the LI magnitude, the β', D_{moon}, α_0, σ, and Ω_{moon} parameters included in (6) and (7) must be known. While β' and D_{moon} can be derived from spacecraft navigation information, the beam misalignment correction term α_0 and the antenna-pattern-related term σ and Ω_{moon} are still required to be determined specifically for each channel of ATMS. The beam alignment bias can be known from measurements during the ground test, but only for three positions at scan angle of ±52° and nadir position. Parameters σ and Ω_{moon} can also be calculated from the antenna pattern. Since there are only four cut measurements of antenna pattern from the ground test for ATMS (0°, 90°, 45°, and 135° direction in azimuth), thus, the calculations of these parameters from the real antenna pattern may not be accurate enough for the LI correction algorithm. To make our model more fitted to ATMS measurement characteristics, the parameters α_0, σ, and Ω_{moon} are determined from (3) by using a best fitting algorithm. The ΔC_{moon} data points used

TABLE II
BEST FIT PARAMETERS FOR ATMS LUNAR CONTAMINATION CORRECTION MODEL

Channel	α_0	δ	Ω_{moon}
1	-0.22	2.23	0.0050
2	-0.38	2.31	0.0053
3	-0.11	0.96	0.0257
4	-0.09	0.95	0.0255
5	-0.10	0.95	0.0258
6	-0.10	0.94	0.0259
7	-0.10	0.93	0.0261
8	-0.11	0.94	0.0262
9	-0.10	0.93	0.0263
10	-0.12	0.92	0.0275
11	-0.14	0.93	0.0277
12	-0.14	0.93	0.0277
13	-0.15	0.94	0.0276
14	-0.16	0.94	0.0277
15	-0.18	0.96	0.0281
16	-0.16	0.90	0.0287
17	-0.25	0.54	0.0913
18	-0.22	0.51	0.0900
19	-0.22	0.51	0.0897
20	-0.22	0.51	0.0894
21	-0.22	0.51	0.0898
22	-0.22	0.50	0.0895

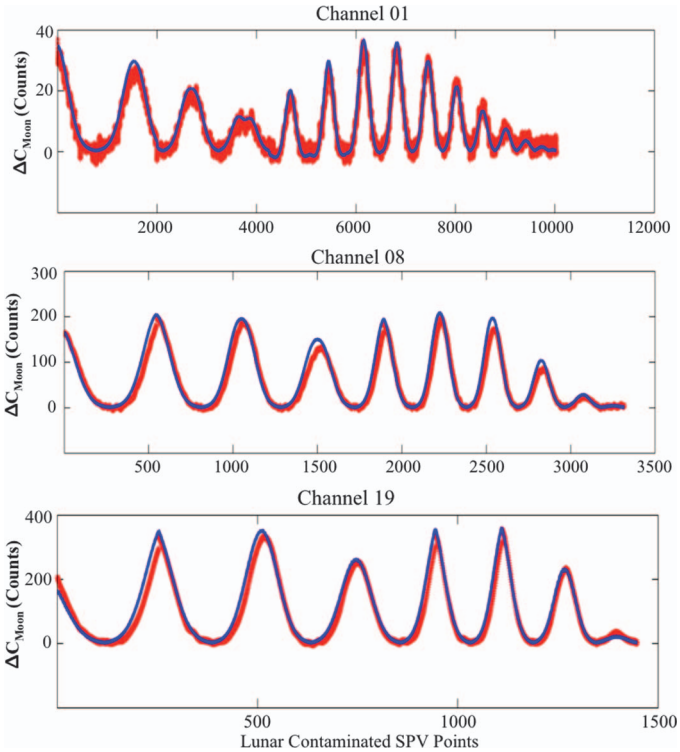

Fig. 7. Comparison of the cold calibration count anomaly (ΔC_{moon}) predicted from lunar model (blue) and observed (red).

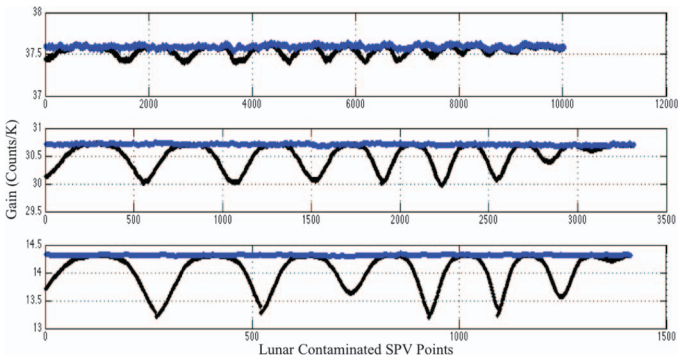

Fig. 8. Comparison of the ATMS calibration gain without lunar contamination corrections at channels 1, 8, and 19 (from top to bottom). Blue lines show the gain after correction and black lines for the gain without the lunar correction.

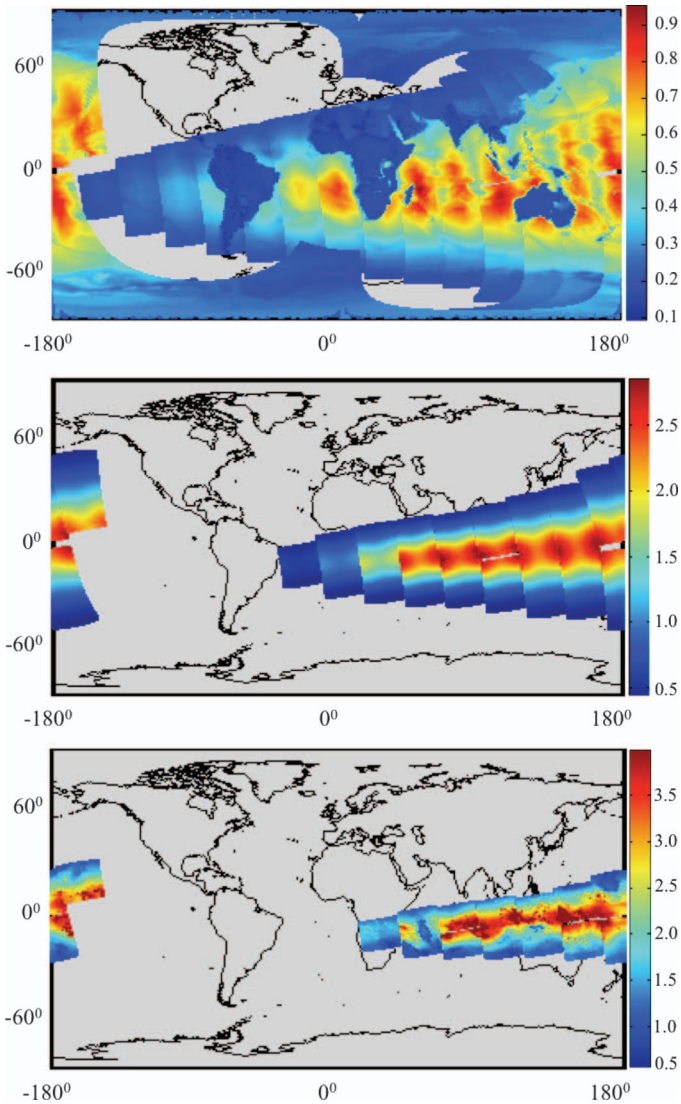

Fig. 9. Scene antenna temperature difference from the lunar contamination corrections for three different ATMS channels at 1, 8, and 19 (from top to bottom) during a 36-h period of lunar intrusion.

for the fitting are extracted from ATMS cold counts, during a complete LI event start and end at 14:00 UTC, on April 19, and at 01:00 UTC, on April 21, 2013. The total of data points being used in the fitting algorithm is 31 277 for the K-band, 8776 for the V-/W-bands, and 3500 for the G-band. The best fitting parameters are listed in Table II. To validate the retrieved parameters, separate data sets of the observed ΔC_{moon}, from 01:00 UTC to 23:59 UTC, on December 05, 2011, are compared with the model prediction. As shown in Fig. 7, the red dots are the observed ΔC_{moon} obtained by using the method described in Section II, and the blue line is the predicted

$\Delta C_{\rm moon}$ by using (4). It can be seen that the model predictions of $\Delta C_{\rm moon}$ agree well with observations at all channels (only representative channels 1, 8, and 17 are shown in Fig. 7).

IV. Assessments of Lunar Contamination Correction Model

A. Model Implementation

As depicted earlier, the LI can be identified by the metric established in Section II, and its intensity can be predicted by (4) in Section III. For ATMS on-orbit calibration in our offline calibration system, the lunar contamination correction model is implemented following these three steps.

Step 1) Calculate the SPV–Moon angle β', the Sun–Moon angle Θ, and the other parameters required by the correction model. Set an LI flag on all four samples of cold counts by using the metric established in (2).

Step 2) For each scan, make an average over the "clean" cold counts, without the LI flag, for use in the calibration equation. If no "clean" cold counts can be found, choose the one with maximum β' value for use in calibration.

Step 3) For a scan with LI flag on it, calculate the cold space brightness temperature increments by using (4), which is matched with the cold count selected in Step 2. The corrected cold space brightness temperature can then be used in a two-point calibration equation.

Without a proper identification and correction of LI, the instrument gain calculated from lunar-contaminated cold counts will become unstable and abnormally deviated from the normal instrument gain. The worst case is when the selected cold count for calibration is with the maximum magnitude of lunar contamination on it, which will be true if there is no filtering for lunar contamination in SPV samples in the calibration process. As shown in Fig. 8, without LI correction, the standard deviation of calibration gain can be as large as 0.31 counts/K, at the G-band, and 0.06/0.22/0.28 counts/K, at the K-/V-/W-bands. After applying the correction model developed in Section III, the anomaly in gain fluctuation arising from lunar contamination is effectively eliminated.

B. Effect of Lunar Contamination on the Scene Antenna Temperature

In reality, it is also very interesting for users to know the impact of LI to the calibration accuracy of ATMS antenna temperature data records (TDRs). From the two-point calibration equation, without considering the nonlinearity of receiver, the TDR calibration error arising from lunar contamination can be expressed as follows:

$$\Delta R = R_s' - R_s = \Delta R_{\rm moon} - \Delta R_{\rm moon} \cdot \left(\frac{C_s - C_c}{C_w - C_c} \right) \quad (8)$$

where R_s and R_s' are calibrated radiances of the earth scene before and after lunar contamination correction, respectively. The terms $\Delta R_{\rm moon}$ are the increments of space view radiance arising from LI. Parameters C_s, C_w, and C_c are the receiver output counts for scene, warm load, and cold space view, respectively. Fig. 9 shows the TDR error in brightness temperature for three different ATMS channels at 1, 8, and 19. It can be seen that the impact of lunar contamination to antenna temperature is channel and scene temperature dependent. As expected by (8), the calibration error increases as scene temperature decreases. For example, at the K-band, the maximum brightness temperature bias is 0.9 K, over ocean, and 0.3 K, over land. The bias increases to 3 K at the V-/W-bands, and this can be as large as 4 K at the G-bands, due to the increased magnitude of LI at these channels.

V. Conclusion

The cold calibration count from the ATMS space view increases when the Moon intrudes the ATMS antenna FOV. This increase is referred to as a lunar contamination since the cold calibration count is not matched with the specified cold space brightness temperature (2.73 K). For ATMS, it is found that the elapse time of LI and the magnitude of the cold count increases are channel dependent. At higher frequency channels with a smaller FOV size such as the G-band, the cold count anomaly arising from LI can be as large as 400. It is also found that the lunar contamination becomes significant only when the Moon appears in the ATMS antenna main beam, and the cold count anomaly can be detected by an angle between space view and lunar observation vectors. A correction model is therefore developed for mitigating the impacts of ATMS LI on calibration. The algorithm has been implemented and validated in our offline calibration system, and it was found to be effective and can be put into operational use in the future.

References

[1] F. Weng, X. Zou, X. Wang, S. Yang, and M. D. Goldberg, "Introduction to Suomi national polar-orbiting partnership advanced technology microwave sounder for numerical weather prediction and tropical cyclone applications," *J. Geophys. Res.*, vol. 117, no. D19, 2012, Art. ID D19112.

[2] F. Weng *et al.*, "Calibration of Suomi national polar-orbiting partnership advanced technology microwave sounder," *J. Geophys. Res.*, vol. 118, no. 19, pp. 1–14, Oct. 2013.

[3] M. Montopoli, A. D. Carlofelice, P. Tognolatti, and F. S. Marzano, "Remote sensing of the moon's subsurface with multifrequency microwave radiometers: A numerical study," *Radio Sci.*, vol. 46, no. 1, 2011, Art. ID RS1012.

[4] B. J. Sandor and R. T. Clancy, "Microwave observations and modelling of a lunar eclipse," *Icarus*, vol. 115, no. 2, pp. 387–398, Jun. 1995.

[5] S. J. Keihm, "Effects of subsurface volume scattering on the lunar microwave brightness temperature spectrum," *Icarus*, vol. 52, no. 3, pp. 570–584, Dec. 1982.

[6] T. Mo and S. Kigawa, "A study of lunar contamination and on-orbit performance of the NOAA 18 advanced microwave sounding unit-A," *J. Geophys. Res.*, vol. 112, 2007, Art. ID D20124.

[7] S. Kigawa and T. Mo, "An algorithm for correction of lunar contamination in AMSU-A data," Nat. Environ. Satellite, Data, Inf. Service, Silver Spring, MD, USA, NOAA Tech. Rep., NESDIS 111, 2002.

[8] F. Weng, H. Yang, and X. Zou, "On convertibility from antenna to sensor brightness temperature for ATMS," *IEEE Geosci. Remote Sens. Lett.*, vol. 10, no. 4, pp. 771–775, Jul. 2013.

[9] Advanced Technology Microwave Sounder (ATMS) calibration data book, Northrop Grumman, Electron. Syst., Falls Church, VA, USA, Rep. 14029B, Mar. 19, 2007.

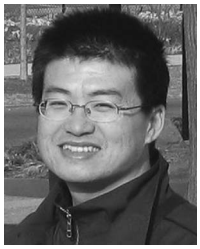

Hu Yang received the Ph.D. degree from the Institute of Remote Sensing Application, China Academy of Science, Beijing, China, in 2003.

His main study field includes passive microwave radiometer calibration/validation, satellite geolocation, and satellite observation simulation. During 2003–2011, he was a Senior Research Scientist in the National Satellite Meteorological Center, China Meteorological Administration, leading microwave instrument calibration and satellite ground application system development as the Instrument Scientist and Program Scientist. Since 2012, he has been with the Earth System Science Interdisciplinary Center (ESSIC), University of Maryland, College Park, MD, USA, working on NPP/JPSS ATMS calibration/validation as project Principal Investigator. He has published over 40 peer-reviewed journals.

Dr. Yang was the winner of the 2010 National Defense Science Advancement Award from the China Aeronautic and Space Agency for his outstanding contribution to the development of China's first spaceborne microwave imager radiometer.

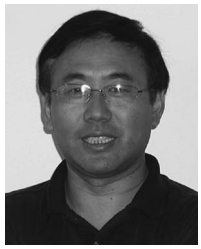

Fuzhong Weng received the Ph.D. degree from Colorado State University, Fort Collins, CO, USA, in 1992.

Currently, he is the Chief of the Sensor Physics Branch, Center for Satellite Applications and Research, NOAA/NESDIS, College Park, MD, USA. In the past 15 years, he has led the developments of NOAA's operational satellite microwave products and algorithms from the Special Sensor Microwave/Imager and the Advanced Microwave Sounding Unit. He is a team member of the National Polar Environmental Satellite Systems microwave operational algorithm. He is the Technical Over Science Lead in developing the community radiative transfer model that has been successfully used in several operational data assimilation systems in the U.S. He has also directly contributed to the developments of microwave land, snow, and sea ice emissivity models which have significantly improved the uses of satellite sounding data in numerical weather prediction (NWP) models. He is currently developing new innovative techniques to advance the uses of satellite measurements under cloudy and precipitation areas in NWP models.